PCCP

RSC Publishing

COMMUNICATION

View Article Online
View Journal | View Issue

Ultrahigh-efficiency photocatalysts based on mesoporous Pt–WO_3 nanohybrids†

Cite this: *Phys. Chem. Chem. Phys.*, 2013, **15**, 6773

Received 13th February 2013,
Accepted 14th March 2013

DOI: 10.1039/c3cp50647a

www.rsc.org/pccp

Zhenhai Wen,[ab] Wei Wu,[ac] Zhuang Liu,[a] Hao Zhang,[a] Jinghong Li*[a] and Junhong Chen*[b]

A reliable nanocasting method has been developed to synthesize mesoporous hybrids of platinum (Pt) nanoparticles decorating tungsten trioxide (WO_3). The process began with modification of the SBA-15 template with carbon polymers and Pt nanoparticles accompanied by adsorption of W^{6+}, which was then converted into m-Pt–WO_3 composites by heat treatment and subsequent template removal. The synthetic strategy can be easily extended to prepare other mesoporous nanohybrids with metal oxide loaded precious metal composites. Comprehensive characterizations suggest that the as-developed m-Pt–WO_3 nanohybrid exhibits unique properties with mesoporous structure, excellent crystalline structure, and high surface area. When the photocatalytic properties of m-Pt–WO_3 nanohybrids were systematically investigated, it was revealed that the m-Pt–WO_3 nanohybrids showed great promise for degrading the organic dye under visible light irradiation, which shows an excellent photocatalytic activity that far exceeded those of pure phase mesoporous WO_3 and commercial TiO_2 (P25), and was 10-fold more active than that of the bulk Pt–WO_3 catalyst. The as-developed synthetic route opens up a new avenue for designing mesoporous hybrid materials for various applications benefiting from the unique porous structure, high surface area, and synergistic effects among constituents.

1. Introduction

Global environmental problems have been a pervasive issue and become more and more serious with the rapid development of industries. Therefore, the development of efficient environmental restoration technologies to address various environmental issues, including air purification, hazardous waste remediation, and self-cleaning, is of great urgency. Photocatalytic technology, which has been demonstrated to enable decomposition of organic contaminants with the assistance of light, represents one of the most promising environmental restoration technologies.[1] However, the present photocatalytic technologies are still far from meeting the demand of practical use due to insufficient photocatalytic efficiency. To date, there have been numerous reports on exploration of novel visible light photocatalysts, such as nitrogen-doped TiO_2, Ag_3PO_4, tungstate, C_3N_4, and bio-inspired compounds, to improve photo-degradation activities.[2] Nonetheless, there are reasons to believe that more research studies are highly required to explore reliable visible-light photocatalysts with high efficiency and good durability.

As an important semiconductor, tungsten oxide (WO_3) has been considered as a potential nontoxic, and stable photocatalyst due to its small band gap (2.4–2.8 eV) as well as high oxidation power of valence band (VB) holes (+3.1–3.2 *vs.* NHE), which makes it possible to efficiently absorb visible light to degrade organic compounds.[3] The only drawback of WO_3 is its relatively low conduction band (CB) edge (+0.3–0.5 *vs.* NHE) that is inadequate for O_2 reduction and can greatly reduce the photocatalytic efficiency due to rapid recombination of the photo-generated holes and electrons.[4] It was reported that this problem can be circumvented by loading platinum (Pt) nanoparticles on WO_3 because the introduction of Pt nanoparticles can promote the multi-electron reduction of oxygen, and thus significantly lessen the recombination effect.[5] Nevertheless, there is still great potential to optimize the Pt–WO_3 composite catalyst associated with its architecture and interactions between Pt and WO_3, because the efficiency of the photocatalyst is highly dependent on the surface area, particle size, morphology or structure, and unique surface characteristics. In particular, photocatalysts with mesoporous structure have great potential to achieve significantly enhanced activities due to their porous structure and large surface area.[6] However, there is still a lack of effective, reliable,

[a] *Beijing Key Laboratory for Analytical Methods and Instrumentation, Tsinghua University, Beijing 100084, China. E-mail: jhli@mail.tsinghua.edu.cn*
[b] *Department of Mechanical Engineering, University of Wisconsin-Milwaukee, 3200 North Cramer Street, Milwaukee, Wisconsin 53211, USA. E-mail: jhchen@uwm.edu*
[c] *Key Laboratory of Jiangxi Province for Ecological Diagnosis-Remediation and Pollution Control, Nanchang Hangkong University, Nanchang 330063, Jiangxi, China*

† Electronic supplementary information (ESI) available. See DOI: 10.1039/c3cp50647a

and versatile methods for fabricating mesoporous metal oxide hybrids with precious metals, despite that such nanohybrids endow great potentiality for exploitation and broad application prospects.[7]

Typically, mesoporous materials can be synthesized through either a soft-template method[8] with liquid crystalline phases as a structure-directing agent or a hard-template route[9] with mesoporous silica or carbon as a framework. Because the synthesis of mesoporous silica is very well established and can be tuned with morphology ranging from noodle-like, rod-like, to spherical shape,[10] mesoporous silica has been widely used as a template for developing other functional mesoporous materials.

We herein describe the use of mesoporous silica as a template in the synthesis of nanohybrid photocatalysts of mesoporous WO_3 loaded Pt nanoparticles (m-Pt–WO_3) with a high specific surface area. The new nanohybrids are conducive for maximizing the utilization of Pt nanoparticles. The as-developed m-Pt–WO_3 exhibited a surprisingly outstanding photocatalytic activity in the photodegradation of methylene blue (blue) dyes with the assistance of visible-light. The synthetic method can be potentially extended to fabricate other mesoporous hybrids with metal oxide loaded highly distributed precious metals.

2. Experimental section

Materials and synthesis

All reagents were of analytical purity and were used without further treatment. Solutions were prepared using Millipore-Q water (>18.0 MΩ cm^{-1}). TiO_2 (P25, 20% rutile and 80% anatase) was purchased from Degussa. SBA-15 was synthesized according to previous reports.[11] In a typical synthesis, 1.0 g of SBA-15 was initially added in a 30 mL aqueous solution containing 0.5 M glucose and 2.0 mM H_2PtCl_6 precursors for 0.5 h. After sonication for half an hour, the mixture was transferred to a 40 mL Teflon-lined stainless steel autoclave and heated at 180 °C for 5 h. After repeated centrifugation and washing three times, the product (C/Pt/SBA-15) was re-dispersed in 30 mL of 0.1 M WCl_6 alcohol solution with continuous stirring at 60 °C until it dried completely. The resulting solid products were then converted to m-Pt–WO_3 nanohybrids after removing SBA-15 templates using 1.0 M of HF solution and burning up carbonaceous polymers at 450 °C for 3 h. Other mesoporous metal oxide hybrid loaded precious metal nanoparticles (PM/MO) can be prepared by simply replacing WCl_6 and H_2PtCl_6 with the corresponding precursors. For comparison, m-WO_3 and Pt/bulk-WO_3 were also prepared. The m-WO_3 could be prepared in a similar way without adding H_2PtCl_6 in the reaction. For the synthesis of Pt/bulk-WO_3, 0.8 g $(NH_4)_2WO_4{\cdot}2H_2O$ was added into 30 mL of 0.5 M glucose solution containing 2.0 mM H_2PtCl_6 with vigorous stirring until it completely dissolved. The mixed solution was then transferred to a 40 mL Teflon-lined stainless steel autoclave and heated at 180 °C for 5 h. Pt/bulk-WO_3 was obtained after annealing the resulting products at 450 °C for 3 h.

Characterization

The samples were characterized using a Hitachi model H-800 transmission electron microscope (TEM) and a JEM 2010 high-resolution transmission electron microscope (HRTEM). X-ray diffraction (XRD) was performed on a Bruker D8-Advance X-ray powder diffractometer. Specific surface areas were obtained through Brunauer–Emmett–Teller (BET) nitrogen adsorption–desorption measurements (Shimadzu, Micromeritics ASAP 2010 Instrument). X-ray photoelectron spectroscopy (XPS) was performed using HP 5950A with MgK_α as the source and the C 1s peak at 284.6 eV as an internal standard.

Photocatalytic experiments

The photocatalytic degradation of methylene blue (MB) dyes was carried out in a homebuilt reactor. Typically, 0.02 g of the catalyst was added to a cylindrical quartz vessel containing 40 mL of the MB solution (0.01 g L^{-1}, *i.e.*, 2.7×10^{-5} mol L^{-1}). A 500 W xenon lamp and a cutoff filter were used as a light source to initiate the reaction (λ > 400 nm; intensity at a wavelength of 420 nm at the catalyst mixture surface was 2000 μW cm^{-2}, estimated with a radiometer, Photoelectronic Instrument Co. IPAS). Before irradiation, the dark adsorption test was adopted to compare the adsorptivity of various catalysts; the mixed solution was kept in the dark for 10 min under stirring. From the difference in the absorbance before and after adsorption, the amount of dyes adsorbed by the catalyst could be estimated. The concentration of the MB solution was monitored based on the absorption spectroscopic technique. The temperature was maintained in the range of 20–25 °C and the pH of the mixed solution was about 6 during the photodegradation. Three consecutive photodegradation experiments were conducted to test the durability of m-Pt/WO_3 catalysts under the same conditions with each cycle lasting for 30 min. The catalysts were recovered through centrifuging, washing, and drying after each cycle, and the refreshed m-Pt/WO_3 catalysts were used for the repeat experiment to degrade MB.

3. Results and discussion

Fig. 1 shows a schematic of the synthetic process for preparing the m-Pt–WO_3 nanohybrids with SBA-15 as the template. Firstly, the nanochannels of mesoporous silica (SBA-15) were modified with a film of carbonaceous polymer embedding Pt nanoparticles (C/Pt/SBA-15) through a well-reported hydrothermal polymerization reaction of glucose.[12] Then, W^{6+} was adsorbed by the formed polymer of nanochannels thanks to the existence of a large number of –OH/–C═O groups. Metal oxide loaded precious metal with a duplicate structure of SBA-15 can be finally achieved after the removal of SBS-15 using HF and the subsequent heat treatment in air.

It is believed that the modification of carbonaceous polymers on the surface of SBA-15 plays a key role in preparation of its replica. On the one hand, the surface properties of the mesoporous silica are highly crucial to achieve uniform and efficient incorporation of targeted material precursors into the

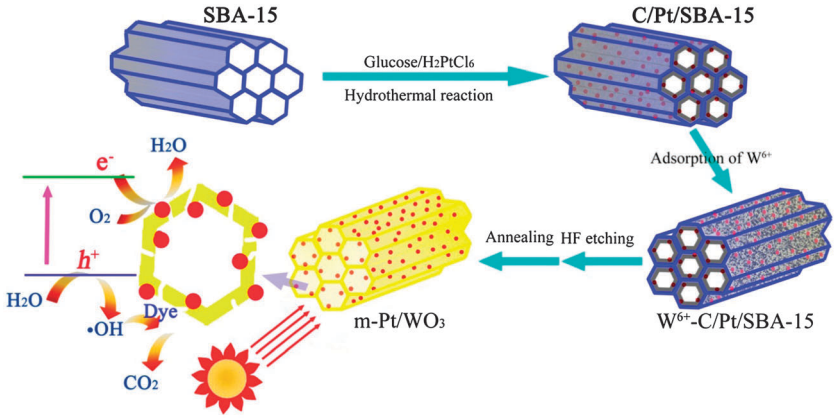

Fig. 1 Illustration of the preparation process of m-Pt/WO_3 and the schematic mechanism of photodegradation of organic dyes by Pt/WO_3 photocatalysts under visible light irradiation.

voids of the template. On the other hand, in contrast to the silicon alkoxides, it is quite difficult to precisely control the hydrolysis or polymerization of most of the metal precursors. The present work takes advantage of recent synthetic advancements in "painting" –OH/–C═O group-rich polymers on the nanochannels of the SBA-15 template. In this way, the precursor can be effectively infiltrated into the pores of the template and subsequently effectively converted to the target material. Moreover, the carbonaceous polymer can function as a reaction reagent for decorating some functional precious metal nanoparticles,[13] and the burning off of the carbonaceous polymer can free up adequate space to accommodate the volume change during the conversion process from precursors to target materials.

In the investigation of the evolving processes, transmission electron microscopy (TEM) was conducted to observe the nanostructures of the products at various stages. By comparing the TEM images of SBA-15 (Fig. 2a), it was clearly demonstrated that a film of carbonaceous polymers was formed with distinct Pt nanoparticles in nanochannels of C–Pt–SBA-15 composites (Fig. 2b). Fig. 2c exhibits a typical TEM image of mesoporous Pt–WO_3 hybrids after removal of the SBA-15 and carbonaceous polymers, which basically maintained the overall morphology of

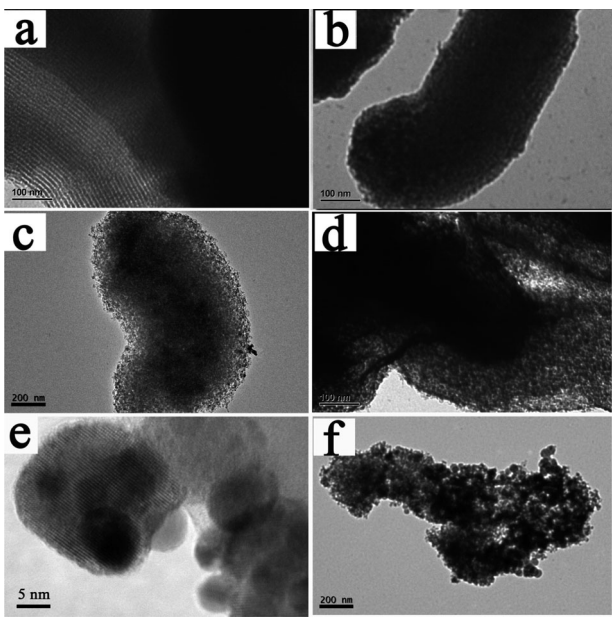

Fig. 2 TEM images of SBA-15 (a), C/Pt/SBA-15 (b), m-Pt/WO_3 free of template (c–e), and m-WO_3 with a different magnification (f).

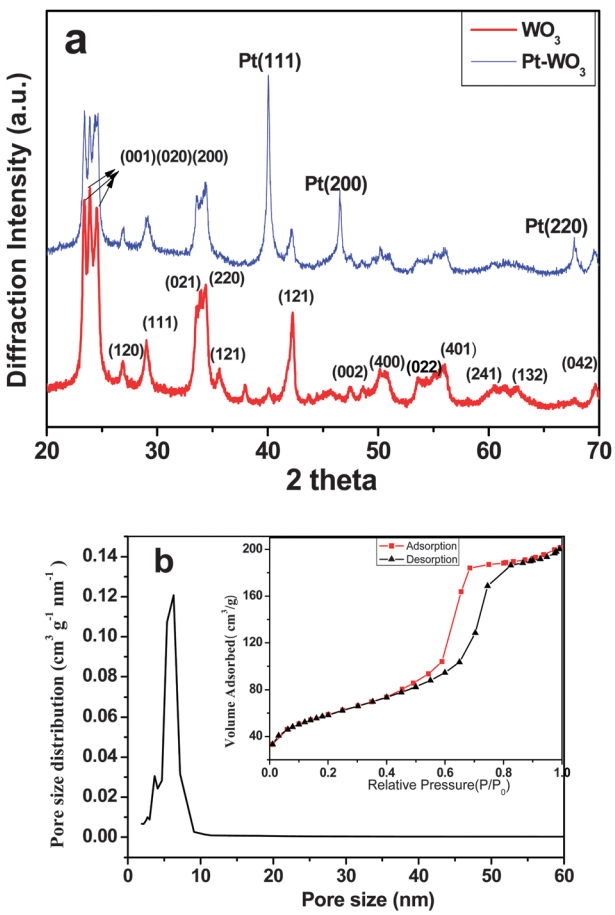

Fig. 3 XRD patterns of m-WO_3 and m-Pt–WO_3 hybrids (a); and pore size distribution and nitrogen adsorption–desorption isotherms (inset) of m-Pt/WO_3 (b).

the well-known monolithic shape of the SBA-15, indicating that the present method can result in a good replicate of the original phase. Fig. 2d presents a representative magnified TEM image of m-Pt–WO_3 hybrids, in which one can clearly observe a disordered porous structure constructed by a large number of nanoparticles in the m-Pt–WO_3 hybrids, which stands in contrast to ordered mesoporous structure in its parent (SBA-15). This result suggests that the ordered structure was partly damaged during the process of removal of the SBA-15 template, burning out of carbonaceous polymers, and formation or growth of crystalline WO_3. It was illustrated that, according to the HRTEM image (Fig. 2e), the WO_3 nanoparticles were decorated with many small Pt nanoparticles. Based on analysis of energy-dispersive X-ray spectroscopy (EDS), it was revealed that the m-Pt/WO_3 comprised of 73.19 wt% W, 21.08 wt% O and 5.73 wt% Pt, respectively (Fig. S1, ESI†). For comparison, we also prepared mesoporous WO_3 (m-WO_3) as a reference sample using a similar method without adding the Pt source during the fabrication process, as shown in Fig. 2f. It is worth mentioning that, besides being used for preparing m-Pt/WO_3 and m-WO_3, the as-developed synthetic strategy can be potentially extended to prepare various mesoporous metal oxides and their composites, which are expected to enhance their performance for practical applications due to their high surface area, tunable pore size, adjustable framework, as well as surface properties. For instance, mesoporous Pt–Fe_2O_3 and Ag–SnO_2 nanohybrids (Fig. S2, ESI†) were also successfully prepared using the same method.

The m-Pt–WO_3 nanohybrids were further characterized for their porous structure, composition, and surface properties. Fig. 3a presents the powder X-ray diffraction (XRD) patterns of m-Pt/WO_3 and m-WO_3, respectively. Well-defined peaks corresponding to (111), (200), and (220) peaks from face-centered cubic (fcc) Pt in m-Pt–WO_3 nanohybrids can be clearly identified. The peaks besides the characteristic peaks of Pt in m-Pt–WO_3 nanohybrids are consistent with the characteristic peak of WO_3, which can be well indexed to the pure monoclinic WO_3 with lattice constants of a = 7.306 Å, b = 7.54 Å, c = 7.692 Å, and β = 90.88° (JCPDS card no. 72-0677). Small-angle X-ray powder diffraction (SXRD) was further performed to characterize the products (Fig. S3, ESI†). The SBA-15 exhibited a typical three-peak pattern corresponding to (10), (11), and (20) reflection lines. In contrast, m-Pt/WO_3 only displayed a feeble broad peak in the range of 1.5–2.5°, suggesting that the evolved m-Pt/WO_3 maintained a porous structure while the highly ordered structure had already collapsed, which is in accordance with structures shown in the TEM images.

The surface area and the porous structure were further investigated through the analysis of nitrogen adsorption–desorption isotherm curves measured at 77 K using the Brunauer–Emmett–Teller (BET) method. m-Pt/WO_3 exhibited a curve of the type IV isotherms with a distinct hysteresis loop at the relative pressure P/P_0 ranging from 0.4 to 0.8 (inset of Fig. 3b), corresponding to different processes between adsorption onto and desorption from the mesopores according to the IUPAC nomenclature. It was demonstrated that m-Pt/WO_3 possessed a BET surface area of 152.7 $m^2\ g^{-1}$, which is one order of magnitude higher than that (9.8 $m^2\ g^{-1}$) of Pt/bulk-WO_3 (Fig. S4, ESI†), and is comparable to that of the mesoporous WO_3

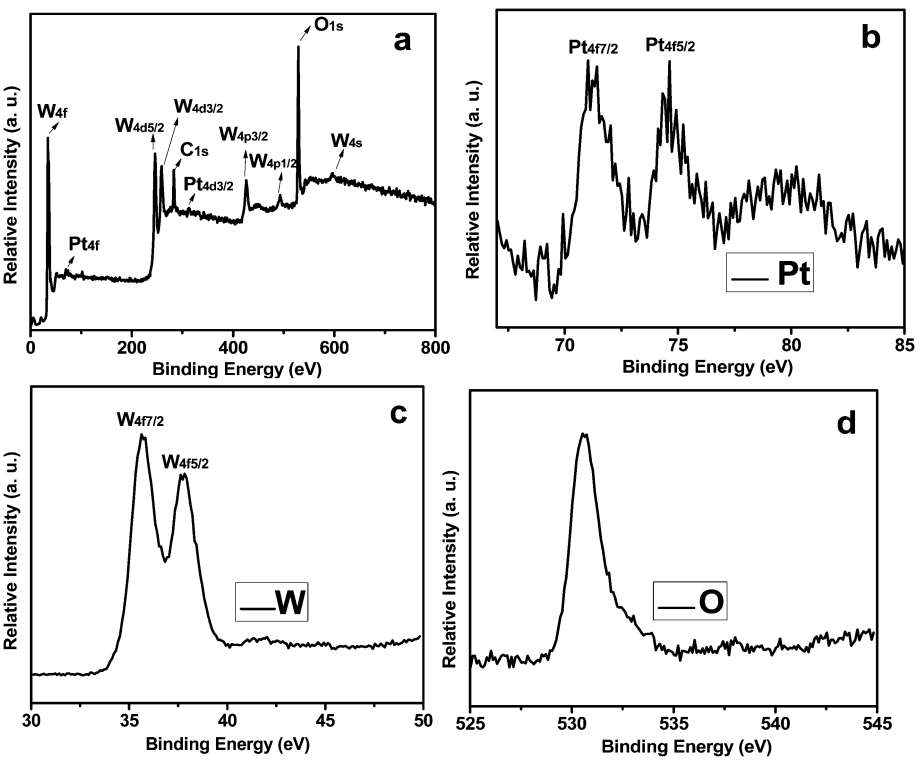

Fig. 4 XPS spectra of m-Pt–WO_3 nanohybrids (a), high-resolution XPS of Pt4f (b), W4f (c) and O 1s in m-Pt/WO_3.

(143.0 m^2 g^{-1}) reported previously.[14] Pore size distributions were calculated from the desorption branch of the N_2 adsorption isotherm using the Barrett–Joyner–Halenda (BJH) formula. As shown in Fig. 3b, m-Pt/WO_3 exhibits a weak peak at 6.3 nm accompanying a feeble peak at about 3.9 nm, indicating the dual-pore structure in the m-Pt–WO_3 hybrids.

The surface composition information of m-Pt/WO_3 was analyzed using X-ray photoelectron spectroscopy (XPS). Fig. 4 presents the survey XPS spectra of m-Pt–WO_3 nanohybrids; one can observe a series of peaks corresponding to W, Pt and O spectra, respectively, confirming the existence of W, Pt, and O elements in m-Pt/WO_3. Fig. 4b–d present high-resolution XPS data of Pt 4f, W 4f, and O 1s in the m-Pt–WO_3 nanohybrids, respectively. One can observe that the 4f7/2 and 4f5/2 signals of Pt are positioned at about 71.1 and 74.3 eV, respectively, suggesting the metallic form (zero valence state) for Pt nanoparticles. Two principal peaks of the W element are centered at 35.4 and 37.6 eV, which can be attributed to the oxidation state of tungsten with +6 valency of the W 4f7/2 and W 4f5/2 spectral lines. The O 1s peak at 530.7 eV is attributed to the oxygen of WO_3. These results are consistent with the XRD pattern results. According to XPS analyses, the m-Pt–WO_3 nanohybrids are comprised of 74.2 wt% W, 19.4 wt% O and 6.4 wt% Pt, respectively.

The photocatalytic activity was obtained by studying photocatalytic oxidation of methyl blue (MB) as a model reaction under visible-light (λ > 400 nm) irradiation with m-Pt/WO_3, Pt/bulk-WO_3 (Fig. S5, ESI†), P25, and m-WO_3 as photocatalysts, respectively. The normalized temporal concentration changes (C/C_0) of MB upon photodegradation were proportional to the normalized maximum absorbance (A/A_0), which can be derived from the changes in the dye's absorption profile (λ = 665 nm) during photocatalytic processes. Fig. 5a presents the temporal concentration changes of MB over different photocatalysts, from which the following fundamental information can be extracted. At first, the MB concentration for various samples decreased in a stepwise manner at different rates during the degradation processes, suggesting that there were remarkable differences in photocatalytic activity among these samples. Secondly, the m-Pt–WO_3 nanohybrids showed a drastic decline in C/C_0 compared with other samples, as evidenced by a C/C_0 value of 0.33 in 2 min, which showed a striking contrast to Pt/bulk-WO_3 that degraded MB to a C/C_0 value of 0.72 within 2 min. Thirdly, almost all MB dyes were degraded in 5 min and 60 min for m-Pt/WO_3 and Pt/bulk-WO_3 catalysts, respectively, while both P25 and m-WO_3 showed an insignificant change even after exposure to visible-light irradiation for 90 min. The photocatalytic activity of these catalysts can also be directly reflected in digital photographs of the MB solution after irradiating with visible light for different durations (Fig. 5b). The m-Pt/WO_3 exhibited a very quick color change from blue, to light blue, and then to colorless during the initial periods, which outperformed the Pt/bulk-WO_3 and was far better than P25 and m-WO_3.

Considering that m-Pt/WO_3 showed much higher photocatalytic activity than Pt/bulk-WO_3 and m-WO_3, it is reasonable

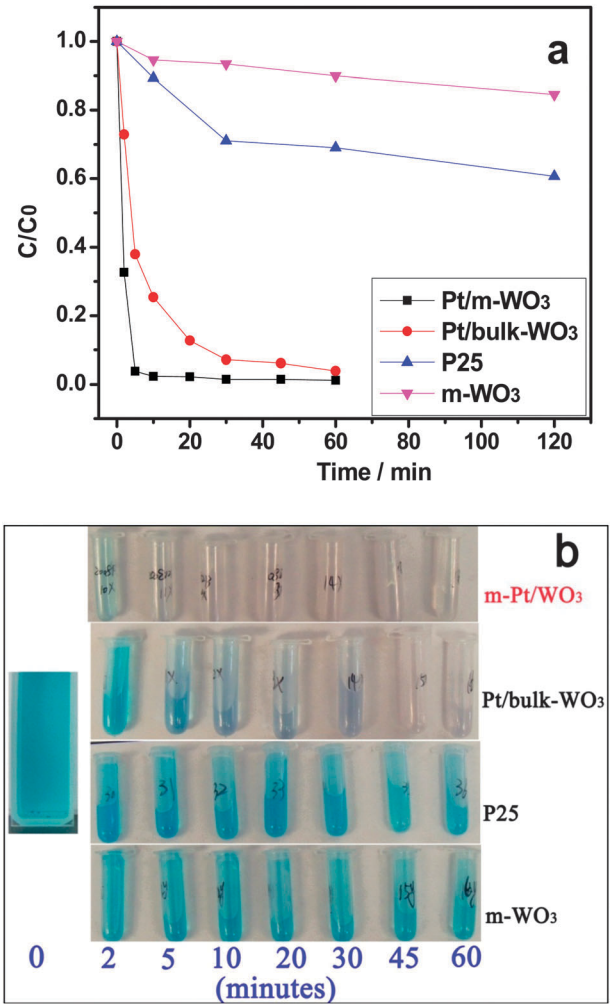

Fig. 5 Concentration variation (a) and digital photographs (b) of the MB solutions during the photodegradation under visible light (λ > 400 nm) over m-Pt/WO_3, Pt/bulk-WO_3, P25, and m-WO_3, respectively.

to conclude that mesoporous structure and loading of Pt nanoparticles are two key factors that improve the photocatalytic activity. It is generally acknowledged that the performance of a photocatalyst is highly dependent on the following three factors, namely the adsorption of dye molecules, the light absorption, and the charge transport and separation.[1a,15] The synergy between Pt nanoparticles and WO_3 can be foreseen to be present in the mesoporous structure due to the porous architecture and interactions between WO_3 and Pt nanoparticles, endowing superior catalytic properties in the as-prepared m-Pt/WO_3. As is well known, the major issue in the WO_3 photocatalyst is the low conduction band (CB) edge (+0.3–0.5 *vs.* NHE), which is not enough to transfer the electron to the oxidant (*e.g.* oxygen), leading to the recombination of photogenerated electrons and holes. One of the effective strategies is to introduce Pt nanoparticles that can efficiently take away the photogenerated electrons and reduce the recombination effect.[5] Obviously, the mesoporous structures can be beneficial to achieve uniform loading of Pt nanoparticles onto the WO_3 surface and thus advance the synergistic effects

between the two components, as was schematically shown in Fig. 1. First, mesoporous structures can effectively absorb more light since the porous structure can enhance the utilization of scattered light;[16] second, the m-Pt/WO_3 may enhance the capability for enrichment of MB on the surface of photocatalysts and offer more catalytic sites for photocatalytic reaction greatly due to the high surface area;[6c,17] third, the Pt nanoparticles are uniformly decorated on the surface of WO_3, which is conducive for achieving optimum performance to make the best of Pt nanoparticles upon suppression of the charge carrier recombination and thus maximizing the performance for degradation of MB. It should be noted that the pure phase m-WO_3 had a similar BET surface area (137.6 $m^2 g^{-1}$) while it displayed a quite weak activity for photodegradation of MB, implying that Pt nanoparticles play a key role in promoting the electron transfer and transport and significantly reduce the charge carrier recombination.[3a]

It should be noted that, in addition to the ultra-high activity, the as-developed m-Pt/WO_3 catalysts also showed excellent stability in repeated running cycles. The durability of the m-Pt/WO_3 catalyst was investigated for the degradation of MB under visible light (Fig. S6, ESI†), which was monitored for three consecutive cycles with a period of 20 min. After each cycle, m-Pt/WO_3 was collected by centrifuging the catalysts used in previous experiments followed by washing and drying, and the fresh MB solution was used for each cycle of photocatalytic experiments. There was no significant change in the photodegradation rate during the three consecutive cycles, and almost all the MB could be degraded in 5 min, indicating the good stability of the prepared m-Pt/WO_3 photocatalyst.

4. Conclusion

In summary, a general and reliable method was developed to prepare various mesoporous structured metal oxide nanohybrids with precious metals. Specifically, m-Pt–WO_3 nanohybrids were synthesized and showed excellent photocatalytic properties with good adsorption capability, better utilization of light, and suppression of charge carrier recombination. The m-Pt–WO_3 nanohybrids show a surprisingly high activity as photocatalysts for degrading organic dyes and exhibited significant improvement in comparison with Pt–bulk-WO_3 hybrids. The superior photocatalytic performance can be ascribed to the mesoporous structures with a considerable surface area and synergistic effects between WO_3 and Pt nanoparticles. This study may open up an attractive avenue for the synthesis of mesoporous nanohybrids for extensive application.

Acknowledgements

This work was financially supported by the National Basic Research Program of China (No. 2011CB935704), the National Natural Science Foundation of China (No. 20903055, No. 21206068, No. 11079002), the Research Fund of Ministry of Education of China (No. 20110002130007), and the U.S. Department of Energy (DE-EE0003208).

References

1 (*a*) A. Kubacka, M. Fernandez-Garcia and G. Colon, *Chem. Rev.*, 2012, **112**, 1555–1614; (*b*) A. Kudo and Y. Miseki, *Chem. Soc. Rev.*, 2009, **38**, 253–278.
2 (*a*) R. Asahi, T. Morikawa, T. Ohwaki, K. Aoki and Y. Taga, *Science*, 2001, **293**, 269–271; (*b*) X. C. Wang, K. Maeda, A. Thomas, K. Takanabe, G. Xin, J. M. Carlsson, K. Domen and M. Antonietti, *Nat. Mater.*, 2009, **8**, 76–80; (*c*) Z. G. Yi, J. H. Ye, N. Kikugawa, T. Kako, S. X. Ouyang, H. Stuart-Williams, H. Yang, J. Y. Cao, W. J. Luo, Z. S. Li, Y. Liu and R. L. Withers, *Nat. Mater.*, 2010, **9**, 559–564; (*d*) C. Huang, C. Li and G. Shi, *Energy Environ. Sci.*, 2012, **5**, 8848–8868; (*e*) Z. Z. Zhang, J. L. Long, L. F. Yang, W. K. Chen, W. X. Dai, X. Z. Fu and X. X. Wang, *Chem. Sci.*, 2011, **2**, 1826–1830.
3 (*a*) J. Kim, C. W. Lee and W. Choi, *Environ. Sci. Technol.*, 2010, **44**, 6849–6854; (*b*) G. R. Bamwenda and H. Arakawa, *Appl. Catal., A*, 2001, **210**, 181–191.
4 (*a*) Y. P. Xie, G. Liu, L. C. Yin and H. M. Cheng, *J. Mater. Chem.*, 2012, **22**, 6746–6751; (*b*) T. Arai, M. Yanagida, Y. Konishi, A. Ikura, Y. Iwasaki, H. Sugihara and K. Sayama, *Appl. Catal., B*, 2008, **84**, 42–47.
5 (*a*) Z. G. Zhao and M. Miyauchi, *Angew. Chem., Int. Ed.*, 2008, **47**, 7051–7055; (*b*) R. Abe, H. Takami, N. Murakami and B. Ohtani, *J. Am. Chem. Soc.*, 2008, **130**, 7780–7081.
6 (*a*) D. S. Wang, Y. D. Duan, Q. Z. Luo, X. Y. Li, J. An, L. L. Bao and L. Shi, *J. Mater. Chem.*, 2012, **22**, 4847–4854; (*b*) K. Kailasam, J. D. Epping, A. Thomas, S. Losse and H. Junge, *Energy Environ. Sci.*, 2011, **4**, 4668–4674; (*c*) A. A. Ismail and D. W. Bahnemann, *J. Mater. Chem.*, 2011, **21**, 11686–11707.
7 Y. Ren, Z. Ma and P. G. Bruce, *Chem. Soc. Rev.*, 2012, **41**, 4909–4927.
8 (*a*) P. D. Yang, D. Y. Zhao, D. I. Margolese, B. F. Chmelka and G. D. Stucky, *Nature*, 1998, **396**, 152–155; (*b*) G. J. A. A. Soler-Illia and O. Azzaroni, *Chem. Soc. Rev.*, 2011, **40**, 1107–1150.
9 (*a*) J. Lee, J. Kim and T. Hyeon, *Adv. Mater.*, 2006, **18**, 2073–2094; (*b*) A. H. Lu and F. Schuth, *Adv. Mater.*, 2006, **18**, 1793–1805.
10 Y. Wan and D. Y. Zhao, *Chem. Rev.*, 2007, **107**, 2821–2860.
11 D. Y. Zhao, J. L. Feng, Q. S. Huo, N. Melosh, G. H. Fredrickson, B. F. Chmelka and G. D. Stucky, *Science*, 1998, **279**, 548–552.
12 Z. H. Wen, J. Liu and J. H. Li, *Adv. Mater.*, 2008, **20**, 743–747.
13 (*a*) X. M. Sun and Y. D. Li, *Angew. Chem., Int. Ed.*, 2004, **43**, 597–601; (*b*) Z. H. Wen, Q. A. Peng, J. P. Zou, G. S. Zeng, S. Q. Ci and J. H. Li, *J. Nanosci. Nanotechnol.*, 2010, **10**, 5723–5729.
14 L. G. Teoh, Y. M. Hon, J. Shieh, W. H. Lai and M. H. Hon, *Sens. Actuators, B*, 2003, **96**, 219–225.
15 (*a*) L. W. Zhang, H. B. Fu and Y. F. Zhu, *Adv. Funct. Mater.*, 2008, **18**, 2180–2189; (*b*) H. Zhang, X. J. Lv, Y. M. Li, Y. Wang and J. H. Li, *ACS Nano*, 2010, **4**, 380–386.
16 M. D. Kelzenberg, S. W. Boettcher, J. A. Petykiewicz, D. B. Turner-Evans, M. C. Putnam, E. L. Warren, J. M. Spurgeon, R. M. Briggs, N. S. Lewis and H. A. Atwater, *Nat. Mater.*, 2010, **9**, 368.
17 J. H. Pan, H. Q. Dou, Z. G. Xiong, C. Xu, J. Z. Ma and X. S. Zhao, *J. Mater. Chem.*, 2010, **20**, 4512–4528.